

Algorithm to solve the time-dependent Schrödinger equation for a charged particle in an inhomogeneous magnetic field: Application to the Aharonov–Bohm effect

Hans De Raedt and Kristel Michielsen

Citation: *Computers in Physics* **8**, 600 (1994); doi: 10.1063/1.168483

View online: <https://doi.org/10.1063/1.168483>

View Table of Contents: <https://aip.scitation.org/toc/cip/8/5>

Published by the [American Institute of Physics](#)

ARTICLES YOU MAY BE INTERESTED IN

[A fast explicit algorithm for the time-dependent Schrödinger equation](#)

Computers in Physics **5**, 596 (1991); <https://doi.org/10.1063/1.168415>

[An accurate and efficient scheme for propagating the time dependent Schrödinger equation](#)

The Journal of Chemical Physics **81**, 3967 (1984); <https://doi.org/10.1063/1.448136>

[The time-dependent Schrödinger equation: Application of absorbing boundary conditions](#)

The Journal of Chemical Physics **90**, 4351 (1989); <https://doi.org/10.1063/1.456646>

[Crank-Nicolson implicit method for the nonlinear Schrodinger equation with variable coefficient](#)

AIP Conference Proceedings **1605**, 76 (2014); <https://doi.org/10.1063/1.4887568>

[Accurate time propagation for the Schrödinger equation with an explicitly time-dependent Hamiltonian](#)

The Journal of Chemical Physics **128**, 184101 (2008); <https://doi.org/10.1063/1.2916581>

[Adaptive Stepsize Runge-Kutta Integration](#)

Computers in Physics **6**, 188 (1992); <https://doi.org/10.1063/1.4823060>



Algorithm to solve the time-dependent Schrödinger equation for a charged particle in an inhomogeneous magnetic field: Application to the Aharonov–Bohm effect

Hans De Raedt and Kristel Michielsen

Institute for Theoretical Physics and Materials Science Centre, University of Groningen,
Nijenborgh4, NL-9747 AG Groningen, The Netherlands

(Received 17 September 1993; accepted 7 April 1994)

This paper introduces an unconditionally stable, accurate, and efficient algorithm to solve the time-dependent Schrödinger equation for a particle moving in an inhomogeneous magnetic field. The algorithm is used to simulate a fundamental thought experiment of quantum mechanics: the magnetic Aharonov–Bohm effect. The calculations demonstrate that the Aharonov–Bohm prediction of the phase shift holds with great precision, even when the dimensions of the interferometer are comparable to the de Broglie wavelength of the particle.

INTRODUCTION

The use of modern circuit lithography has made it possible to manufacture solid-state devices of submicrometer dimensions. Electrons can cross such systems before their motion is disturbed by crystal impurities or other scattering mechanisms and travel “ballistically” very much like electrons in vacuum do. This then opens the possibility of performing electron-optics experiments in solid-state devices and, eventually, of making solid-state switches that use the wave-mechanical nature of the electron motion.

Once the characteristic length scale of the device becomes comparable to the wavelength of the electrons, theoretical methods of analysis such as geometrical (ray) optics or semiclassical approximations can no longer be justified.¹ Then a proper theoretical description of the single-particle physics requires the solution of the Schrödinger equation. Computer simulation has proven to be a useful tool to gain insight into various aspects of electron motion in nanoscale devices.^{2,3} Among other things it has shown that under the stringent conditions mentioned above, semiclassical notions about for instance tunneling times or electron collimation do not survive a confrontation with numerical facts.^{4,5}

In experiments, a magnetic field is often used to probe the properties of a particular device. Also there is considerable experimental interest in metal-superconductor devices. Clearly in these systems the magnetic field is inhomogeneous: Far enough inside the superconductor it is zero whereas in the metal it is not. The purpose of this paper is to introduce a numerical algorithm to solve the time-dependent Schrödinger equation (TDSE) for a particle moving in an inhomogeneous magnetic field. The algorithm uses a product formula, recently introduced by Suzuki.⁶ The method is numerically stable and convergent under all circumstances. Moreover it is accurate to fourth order in both the spatial and temporal mesh size, efficient and well suited for implementation on scalar, vector and parallel computer architectures. In general, the TDSE approach is flexible in the sense that it can handle arbitrary geometries and (vector) potentials and therefore provides a unified

framework to investigate various physical problems.

The emphasis of this paper will be on the algorithm and its application to a fundamental thought experiment of quantum mechanics: Scattering of charged particles by two slits, in the presence of a magnetic field restricted to a region from which the electrons are excluded (see Fig. 1, taken from Ref. 7). Applications to mesoscopic metal-superconductor devices will be presented elsewhere.

Many textbooks (for a very short list see Refs. 7–10) on quantum mechanics use this example to introduce the concept of the Aharonov–Bohm (AB) effect.¹¹ As far as we know, a (numerically) exact solution of the corresponding Schrödinger problem has not been given. This example provides a stringent test of the algorithm. Usually, in theoretical treatments of the AB effect, it is assumed that the electron beam can be split into two beams, the trajectories of which are dominantly classical.^{10–12} The simulation technique can be used to explore situations in which this assumption cannot be made: The case where the dimensions of the interferometer (the two slits) are comparable to the wavelength of the particle. Under these circumstances the diffraction patterns (shown below) cannot be fitted by the expression obtained in the semiclassical limit.⁸ However, as will be shown below, only minor modifications are required to get excellent agreement with the (numerically) exact results.

I. ALGORITHM: THEORY

The approach taken in this paper is to simulate the motion of the particle by numerically solving the TDSE

$$i\hbar \frac{\partial}{\partial t} |\Phi(t)\rangle = \mathcal{H} |\Phi(t)\rangle, \quad (1.1)$$

where $|\Phi(t)\rangle$ represents the state of the system described by the Hamiltonian \mathcal{H} . The formal solution of the TDSE is given by

$$|\Phi(m\tau)\rangle = e^{-im\tau\mathcal{H}} |\Phi(t=0)\rangle, \quad (1.2)$$

where $m=0,1,\dots$ counts the number of time-steps τ .

For the present and future applications it is expedient to develop an algorithm that is correct up to fourth order, both in space and time. The accuracy of this algorithm is high whereas computational effort required remains reasonable (see below). The key concept in the construction of an unconditionally stable algorithm for solving the TDSE is the use of a unitary approximation to the time-step operator $U(\tau) = e^{-i\tau\mathcal{H}}$.¹³ Product formulas provide a convenient framework to construct such approximations.¹³ Procedures to devise algorithms that are correct up to fourth order in the time step are given in Ref. 13. From practical point of view, a disadvantage of the fourth-order methods introduced in Ref. 13 is that they involve commutators of various contributions to the Hamiltonian. Recently Suzuki proposed a symmetrized fractal decomposition of the time evolution operator.¹⁴ Using Suzuki's formula, a fourth-order algorithm is easily built from a second-order algorithm by applying formula¹⁴

$$U_4(\tau) = U_2(p\tau)U_2(p\tau)U_2[(1-4p)\tau]U_2(p\tau)U_2(p\tau), \quad (1.3)$$

where $p=1/(4-4^{1/3})$ and $U_n(\tau)$ is an n th order unitary approximation to $U(\tau)$, i.e., $U(\tau)=U_n(\tau)+\mathcal{O}(\tau^{n+1})$. Approximants correct up to second order are obtained by symmetrization of first order approximants,^{13,15,16} namely

$$U_2(\tau) = U_1^T(\tau/2)U_1(\tau/2), \quad (1.4)$$

where the U_1^T is the transpose of U_1 .

Usually the Hamiltonian can be written as a sum of different contributions which may or may not commute. The first-order approximant $U_1(\tau)$, corresponding to the decomposition

$$\mathcal{H} = \sum_{n=1}^N \mathcal{H}_n, \quad (1.5a)$$

is given by

$$U_1(\tau) = e^{-i\tau\mathcal{H}_1}e^{-i\tau\mathcal{H}_2}\dots e^{-i\tau\mathcal{H}_N} = \prod_{n=1}^N e^{-i\tau\mathcal{H}_n}. \quad (1.5b)$$

In general there will be many possibilities to write down different decompositions of a given Hamiltonian. From theoretical point of view, the choice of the decomposition is arbitrary. In practice however, this flexibility can be exploited to considerable extent to tailor the algorithm to the computer architecture on which the algorithm will execute. Of particular interest are decompositions that vectorize extremely well and have a large intrinsic degree of parallelism.

Having reached a point where it is impossible to proceed with formal manipulations only, it is nevertheless important to recognize that for any decomposition Eq. (1.5a) of \mathcal{H} , the use of the unitary operator $U_1(\tau)$ guarantees that the algorithm defined by Eq. (1.3) is unconditionally stable and correct up to fourth order in the time step.

The Hamiltonian of a charged (spinless) nonrelativistic particle in an external, static magnetic field \mathbf{B} reads

$$\mathcal{H} = \frac{1}{2m^*} (\mathbf{p} - e\mathbf{A})^2 + V, \quad (1.6)$$

where m^* is the effective mass of the particle with charge e , $\mathbf{p} = -i\hbar\nabla$ is the momentum operator, \mathbf{A} represents the vector potential, and V denotes the potential. The simplest realization of the AB thought experiment¹¹ corresponds to the choice $\mathbf{B}=[0, 0, B(x,y)]$ and $V=V(x,y)$. Then the problem is essentially two-dimensional and the motion of the particle may be confined to the $x-y$ plane. The potential $V(x,y)$ will be used to specify the geometry of the interferometer. For numerical work, there is no compelling reason to adopt the Coulomb gauge ($\text{div } \mathbf{A}=0$). A convenient choice for the vector potential is $\mathbf{A}=[A_x(x,y), 0, 0]$, where

$$A_x(x,y) = - \int_0^y B(x,y) dy. \quad (1.7)$$

We will solve the TDSE Eq. (1.1) with Hamiltonian Eq. (1.6) with the boundary condition that the wave function is zero outside the simulation box, i.e., we assume perfectly reflecting boundaries.

For computational purposes it is expedient to express all quantities in dimensionless units. Fixing the unit of length by λ , wave vectors are measured in units of $k=2\pi/\lambda$, energies in $E=\hbar^2 k^2/2m^*$, time in \hbar/E and vector potential in units of $e\lambda/\hbar$. Expressed in these dimensionless variables Hamiltonian Eq. (1.6) reads

$$\mathcal{H} = -\frac{1}{4\pi^2} \left[\left(\frac{\partial}{\partial x} - iA_x(x,y) \right)^2 + \frac{\partial^2}{\partial y^2} \right] + V(x,y). \quad (1.8)$$

An essential step in the construction of a numerical algorithm is to discretize the derivatives with respect to the x and y coordinates. For our purposes, it is necessary to use a difference formula for the first and second derivatives in Eq. (1.8) that is accurate up to fourth order in the spatial mesh size δ . Using the standard four and five point difference formula¹⁷ the discretized rhs of Eq. (1.8) reads

$$\begin{aligned} \mathcal{H}\Phi_{l,k}(t) = & \frac{1}{48\pi^2\delta^2} \left\{ [1 - i\delta(A_{l,k} + A_{l+2,k})]\Phi_{l+2,k}(t) + [1 + i\delta(A_{l-2,k} + A_{l,k})]\Phi_{l-2,k}(t) \right. \\ & - 16 \left[1 - \frac{i\delta}{2} (A_{l,k} + A_{l+1,k}) \right] \Phi_{l+1,k}(t) - 16 \left[1 + \frac{i\delta}{2} (A_{l-1,k} + A_{l,k}) \right] \Phi_{l-1,k}(t) \\ & \left. + \Phi_{l,k+2}(t) + \Phi_{l,k-2}(t) - 16\Phi_{l,k+1}(t) - 16\Phi_{l,k-1}(t) + (60 + \delta^2 A_{l,k}^2 + 48\pi^2\delta^2 V_{l,k})\Phi_{l,k}(t) \right\} + \mathcal{O}(\delta^5), \end{aligned} \quad (1.9)$$

where $\Phi_{l,k}(t) = \Phi(l\delta, k\delta, t)$ and $A_{l,k} = A_x(l\delta, k\delta)$. The discretized form Eq. (1.9) will provide a good approximation to the continuum problem, if δ is substantially smaller than the smallest physical length scale. For the case at hand there are two

such scales. One is the de Broglie wavelength of the particle (which by definition is equal to λ) and the other is the (smallest) magnetic length defined by $l_B^2 = \min_{B(x,y)} |\hbar/eB(x,y)|$. From numerical calculations (not shown) it follows that $\delta=0.1 \min(1, l_B)$ yields a good compromise between accuracy and the CPU time required to solve the TDSE.

Straightforward application of the product-formula recipe to expression (1.9) requires a cumbersome matrix notation. This can be done more elegantly in the following way.¹³ Defining

$$|\Phi(t)\rangle = \sum_{l=1}^{L_x} \sum_{k=1}^{L_y} \Phi_{l,k}(t) c_{l,k}^+ |0\rangle, \quad (1.10)$$

where L_x and L_y are the number of grid points in the x and y direction, respectively, and $c_{l,k}^+$ creates a particle at lattice site (l,k) , Eq. (1.10) can be written as

$$|\Phi(m\tau)\rangle = e^{-im\tau H} |\Phi(t=0)\rangle, \quad (1.11)$$

where

$$\begin{aligned} H = & \frac{1}{48\pi^2\delta^2} \sum_{l=1}^{L_x-2} \sum_{k=1}^{L_y} \{ [1 - i\delta(A_{l,k} + A_{l+2,k})] c_{l,k}^+ c_{l+2,k} + [1 + i\delta(A_{l,k} + A_{l+2,k})] c_{l+2,k}^+ c_{l,k} \} - \frac{1}{3\pi^2\delta^2} \\ & \times \sum_{l=1}^{L_x-1} \sum_{k=1}^{L_y} \left\{ \left[1 - \frac{i\delta}{2} (A_{l,k} + A_{l+1,k}) \right] c_{l,k}^+ c_{l+1,k} + \left[1 + \frac{i\delta}{2} (A_{l,k} + A_{l+1,k}) \right] c_{l+1,k}^+ c_{l,k} \right\} + \frac{1}{48\pi^2\delta^2} \\ & \times \sum_{l=1}^{L_x} \sum_{k=1}^{L_y-2} (c_{l,k}^+ c_{l,k+2} + c_{l,k+2}^+ c_{l,k}) - \frac{1}{3\pi^2\delta^2} \sum_{l=1}^{L_x} \sum_{k=1}^{L_y-1} (c_{l,k}^+ c_{l,k+1} + c_{l,k+1}^+ c_{l,k}) + \frac{1}{48\pi^2\delta^2} \\ & \times \sum_{l=1}^{L_x} \sum_{k=1}^{L_y} (60 + \delta^2 A_{l,k}^2 + 48\pi^2\delta^2 V_{l,k}) + \mathcal{O}(\delta^5), \end{aligned} \quad (1.12)$$

where $c_{l,k}$ annihilates a particle at lattice site (l,k) .

Hamiltonian Eq. (1.12) describes a particle that moves on a two-dimensional lattice by making nearest and next-nearest neighbor jumps. This interpretation suggests that H should be written as a sum of terms that represent groups of independent jumps.¹³ A convenient choice is

$$\begin{aligned} H_1 = & \frac{1}{48\pi^2\delta^2} \sum_{l \in X_1} \sum_{k=1}^{L_y} \{ [1 - i\delta(A_{l,k} + A_{l+2,k})] c_{l,k}^+ c_{l+2,k} \\ & + [1 + i\delta(A_{l,k} + A_{l+2,k})] c_{l+2,k}^+ c_{l,k} \}; \end{aligned}$$

$$X_1 = \{1, 2, 5, 6, 9, 10, \dots\},$$

$$\begin{aligned} H_2 = & \frac{1}{48\pi^2\delta^2} \sum_{k=1}^{L_y} \sum_{l \in X_2} \{ [1 - i\delta(A_{l,k} + A_{l+2,k})] c_{l,k}^+ c_{l+2,k} \\ & + [1 + i\delta(A_{l,k} + A_{l+2,k})] c_{l+2,k}^+ c_{l,k} \}; \end{aligned}$$

$$X_2 = \{3, 4, 7, 8, 11, 12, \dots\},$$

$$\begin{aligned} H_3 = & \frac{-1}{3\pi^2\delta^2} \sum_{k=1}^{L_y} \sum_{l \in X_3} \left\{ \left[1 - \frac{i\delta}{2} (A_{l,k} + A_{l+1,k}) \right] c_{l,k}^+ c_{l+1,k} \right. \\ & \left. + \left[1 + \frac{i\delta}{2} (A_{l,k} + A_{l+1,k}) \right] c_{l+1,k}^+ c_{l,k} \right\}; \end{aligned}$$

$$X_3 = \{1, 3, 5, 7, 9, 11, \dots\},$$

$$\begin{aligned} H_4 = & \frac{-1}{3\pi^2\delta^2} \sum_{k=1}^{L_y} \sum_{l \in X_4} \left\{ \left[1 - \frac{i\delta}{2} (A_{l,k} + A_{l+1,k}) \right] c_{l,k}^+ c_{l+1,k} \right. \\ & \left. + \left[1 + \frac{i\delta}{2} (A_{l,k} + A_{l+1,k}) \right] c_{l+1,k}^+ c_{l,k} \right\}; \end{aligned}$$

$$X_4 = \{2, 4, 6, 8, 10, 12, \dots\},$$

$$H_5 = \frac{1}{48\pi^2\delta^2} \sum_{k \in X_5} \sum_{l=1}^{L_x} (c_{l,k}^+ c_{l,k+2} + c_{l,k+2}^+ c_{l,k}); \quad (1.13)$$

$$X_5 = \{1, 2, 5, 6, 9, 10, \dots\},$$

$$H_6 = \frac{1}{48\pi^2\delta^2} \sum_{k \in X_6} \sum_{l=1}^{L_x} (c_{l,k}^+ c_{l,k+2} + c_{l,k+2}^+ c_{l,k});$$

$$X_6 = \{3, 4, 7, 8, 11, 12, \dots\},$$

$$H_7 = \frac{-1}{3\pi^2\delta^2} \sum_{k \in X_7} \sum_{l=1}^{L_x} (c_{l,k}^+ c_{l,k+1} + c_{l,k+1}^+ c_{l,k});$$

$$X_7 = \{1, 2, 5, 6, 9, 10, \dots\},$$

$$H_8 = \frac{-1}{3\pi^2\delta^2} \sum_{k \in X_8} \sum_{l=1}^{L_x} (c_{l,k}^+ c_{l,k+1} + c_{l,k+1}^+ c_{l,k});$$

$$X_8 = \{3, 4, 7, 8, 11, 12, \dots\},$$

$$H_9 = \frac{1}{48\pi^2\delta^2} \sum_{k=1}^{L_y} \sum_{l=1}^{L_x} (60 + \delta^2 A_{l,k}^2 + 48\pi^2\delta^2 V_{l,k}),$$

and

$$U_1(\tau) = \prod_{n=1}^9 e^{-i\tau H_n}, \quad (1.14)$$

is the first-order approximant from which the algorithm, correct up to fourth order in the spatial (δ) and temporal (τ) mesh size, can be built.

Inspection of H_n for $n=1,\dots,9$ shows that each of the terms in the curly brackets commutes with all the other terms in the sum over k and l . This is because each of these terms corresponds to a jump of the particle between a pair of two, isolated sites. For the purpose of implementation, this feature is of extreme importance.¹³ To illustrate this point it is sufficient to consider the first of the exponents in Eq. (1.14) and use the fact that all terms commute to rewrite it as

$$e^{-i\tau H_1} = \prod_{k=1}^{L_y} \prod_{l \in X_1} \exp\left(\frac{-i\tau}{48\pi^2\delta^2} \{[1 - i\delta(A_{l,k} + A_{l+2,k})] \times c_{l,k}^+ c_{l+2,k}^- + [1 + i\delta(A_{l,k} + A_{l+2,k})] c_{l+2,k}^+ c_{l,k}^-\}\right). \quad (1.15)$$

Furthermore, as each of the exponents in the product (1.15) is merely describing a two-site system, the exponent of the two-by-two matrix can be worked out analytically.¹³ In general

$$\begin{aligned} & \exp(\tau\alpha c_{l,k}^+ c_{l',k'}^- + \tau\alpha^* c_{l',k'}^+ c_{l,k}^-) \\ &= (c_{l,k}^+ c_{l',k'}^- + c_{l',k'}^+ c_{l,k}^-) \cos \tau|\alpha| - i \\ & \quad \times (\alpha^{*-1} c_{l,k}^+ c_{l',k'}^- + \alpha^{-1} c_{l',k'}^+ c_{l,k}^-) \sin \tau|\alpha|. \end{aligned} \quad (1.16)$$

Fortunately, the rather formal language used above is easily translated into a computer program. All that Eqs. (1.13)–(1.16) imply is that for each factor in product formula (1.14) one has to pick successive pairs of lattice points, get the values of the wave function at each pair of points and perform a plane rotation using matrices of the form

$$M = \begin{pmatrix} \cos \tau|\alpha| & -i\alpha^{-1} \sin \tau|\alpha| \\ -i\alpha^{*-1} \sin \tau|\alpha| & \cos \tau|\alpha| \end{pmatrix}. \quad (1.17)$$

For each of the nine exponentials,¹⁸ the order in which the pairs of points are processed is irrelevant. Therefore, the computation of each of the nine factors can be done entirely parallel, fully vectorized, or mixed parallel and vectorized depending on the computer architecture on which the code will execute.

II. ALGORITHM: IMPLEMENTATION

Implementation of the algorithm is relatively simple. As an example, a FORTRAN program that computes $e^{i\tau H_1}|\Psi\rangle$ is given below. The real and imaginary part of the wave function are held in $\text{psi}(2i-1)$ and $\text{psi}(2i)$, respectively. The arrays $\text{cnnn}(i)$, $\text{snnn}(i)$, and $\text{rnnn}(i)$, are used to hold $\cos \tau[1 - i\delta(A_{l,k} + A_{l+2,k})]$, $\sin \tau[1 - i\delta(A_{l,k} + A_{l+2,k})]$, and $\delta(A_{l,k} + A_{l+2,k})[1 - i\delta(A_{l,k} + A_{l+2,k})]$, and $\sin \tau[1 - i\delta(A_{l,k} + A_{l+2,k})]$, respectively. Of course, using these arrays costs memory. If memory usage would cause

problems, the variables c , s , and $r4$ can be calculated in place. On the CRAY YMP this increases the CPU time used by the whole program by a factor of 2;

```
c = exp(-i\tau H_1), x_1
do n=1,3,2
do j=0,2*Lx*Ly-1,Lx+Lx
k=j/2-3
do i=j+n, j+Lx+Lx-5, 8
k=k+4
c=cnnn(k)
s=snnn(k)
r4=rnnn(k)
r0=psi(i)
r1=psi(i+1)
psi(i)=r0*c+psi(i+5)*s+psi(i+4)*r4
psi(i+1)=r1*c-psi(i+4)*s+psi(i+5)*r4
psi(i+4)=psi(i+4)*c+r1*s-r0*r4
psi(i+5)=psi(i+5)*c-r0*s-r1*r4
enddo
enddo
enddo
```

This code autovectorizes and autotasks on the CRAY YMP, and executes at a cruising speed of 200 Mflops per processor (as do the codes that perform the calculations for H_2, \dots, H_9). When it is run on more than one processor, there seems to be no significant loss of performance. Also on super-scalar processors such as the one in the IBM RS/6000, the whole program executes at a speed which is close to the theoretical limit of the particular machine. For zero magnetic field the new code reproduces the numbers generated by the old algorithm.¹³ Preliminary work on porting the code to the CM5 indicates that it will be possible to reach an efficiency of about 25% of the theoretical speed limit of that machine.

III. APPLICATION: AHARONOV-BOHM EFFECT

In classical mechanics the motion of a charged particle is not affected by the presence of electromagnetic fields in regions from which the particle is excluded. In classical physics the vector potential $\mathbf{A}=(A_x, A_y, A_z)$ and scalar potential are merely convenient mathematical tools from which the electric and magnetic fields may be calculated.

In quantum physics the vector potential does acquire physical significance. According to Aharonov and Bohm,¹¹ the vector potential itself can lead to measurable effects even though the particle never enters the region where the electromagnetic field is nonzero. AB predict an observable phase shift of the particles wave packet. The existence of the AB effect and the interpretation of experiments designed to confirm its existence have been the subject of a long debate. A comprehensive review of the different viewpoints and experimental results is given in Ref. 19. Additional information can be found in Refs. 20, 21. Ingenious experiments^{22,23} and theoretical work²⁴ have given further support to the existence of the AB effect.

Although there seems to be a general consensus that the AB effect does exist, theoretical modeling of many of the actual or thought experiments is not as simple as it may seem. Often there are (hidden) *ad hoc* assumptions and simplifications that require additional analysis, such as the use of semiclassical approximations.^{10–12} The numerical thought experiment (see Fig. 1) reported on in this paper is free from all kinds of ambiguities but is, for obvious practical reasons, less realistic from experimental point of view.

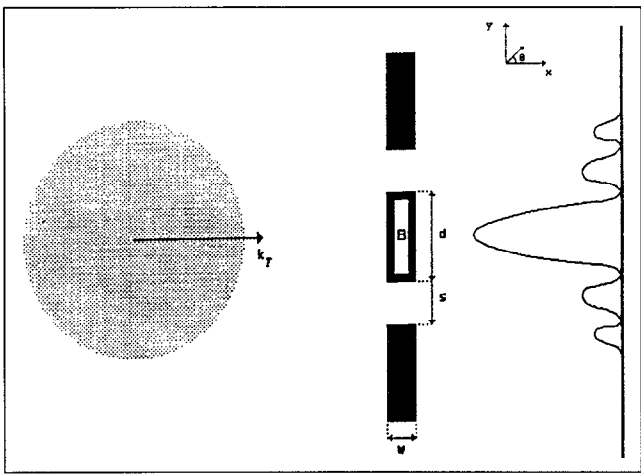


Figure 1. Layout of the two-slit interferometer. The initial wave packet, shown on the left of the two slits, moves to the right and is partially transmitted by the two slits of width s . The transmitted wave yields an interference pattern on a screen placed (far) to the right of the interferometer. The magnetic field B is nonzero in the interior of the center block.

In recent years, the term AB effect is used in a more general context than the one described above. It is now common to invoke the concept of the AB phenomenon if a measurable property of a system appears to depend on the magnetic flux through the system. This has proven to be very useful to interpret many experiments on mesoscopic rings and other structures.^{25,26} Clearly, it is straightforward to use the simulation technique introduced here to study for instance rings or junctions (this merely requires putting in the appropriate potential) but this is out of the scope of the present paper.

The geometry of the two-slit apparatus is defined by three spatial regions of very large potential ($V \gg E$), as indicated in Fig. 1. Well within the middle block a local, but otherwise constant, magnetic field $\mathbf{B}=[0,0,B(x,y)]$ is present. The magnetic field is shielded from the free-space region by a 2δ thick wall of potential V . For $V=100E$ the total, accumulated (in time) intensity inside the three blocks, is less than 10^{-9} , which is below the numerical noise of the simulation itself. Therefore, for all purposes, the electron wave packet does not “feel” the magnetic field inside the middle block.

Most calculations have been carried out using the vector potential

$$\mathbf{A}=[A_x(y),0,0], \quad (2.1)$$

where $A_x(y)=-\int_0^y B(x,y')dy'$. Some calculations have been repeated using $\mathbf{A}=[0,A_y(x),0]$ and, as required by gauge invariance, the numerical results of the probability distribution are the same.

According to AB ,¹¹ the phase shift of the diffraction pattern is given by

$$\varphi=\frac{e}{\hbar}\int \mathbf{B} \cdot d\mathbf{S}, \quad (2.2)$$

or, using the units adopted in this paper,

$$\frac{B}{\text{Tesla}}=437\varphi \frac{m^*}{m_e} \frac{E}{eV} \frac{\lambda^2}{S}, \quad (2.3)$$

where $S=(w-4\delta)(d-4\delta)$ is the area in which $\mathbf{B} \neq 0$, and m_e denotes the electron mass.

The condition for a maximum shift is $\varphi=(2k+1)\pi$, for $k=0,\pm 1,\dots$. Taking $k=0$ and calling the corresponding magnetic field B_0 the phase shift can be written as

$$\frac{\varphi}{\pi}=\frac{B}{B_0}. \quad (2.4)$$

For numerical purposes, this is a convenient way of expressing the strength of the magnetic field. Typical values for GaAs devices are $E=0.021$ eV, $\lambda=335$ Å, $m^*/m_e=0.067$ yielding $B/T \approx 1.9\varphi/\pi S$.

Conceptually, the simulation procedure is rather simple. First the initial wave packet is positioned far to the left of the two-slit interferometer. A convenient choice is

$$\Phi(x,y) \propto e^{2\pi i k(x \cos \theta_0 + y \sin \theta_0)} e^{-(x-x_0)^2/2\sigma_x^2} e^{-(y-y_0)^2/2\sigma_y^2}, \quad (2.5)$$

i.e., a Gaussian wave packet centered around (x_0, y_0) with energy $\langle \Phi | \mathcal{H} | \Phi \rangle = E$ and width σ_x and σ_y in the x and y direction, respectively. In free space wave packet Eq. (2.5) moves in the $(\cos \theta_0, \sin \theta_0)$ direction. In practice, a spatial window is used to truncate the Gaussian. The resulting initial wave packet is normalized such that $\int |\Phi(x,y)|^2 dx dy = 1$. The effect of this approximation shows up in the sixth digit of the energy and momentum of the wave packet, in other words it is negligible. Taking $\sigma_x = \sigma_y = 6\lambda$ yields a Gaussian packet that is a good approximation to a plane wave (in this case) and can still be accommodated by a simulation box ($1024\lambda \times 511\lambda$) of reasonable size. Note that the existence of the AB effect does not depend on the particular choice of the wave packet, but is a result of the topology of the potential and the presence of a vector potential.¹¹

The second step is to solve the TDSE, using the numerical technique outlined above. In all calculations the spatial mesh size $\delta=0.1\lambda$ and the time step $\tau=0.03125\hbar/E$. It takes at least 5120 time steps before the scattering of the wave by the two-slit potential becomes negligible. A typical run takes about 4 h of CPU time on the CRAY YMP, using a single processor. Increasing the size of the system and of the initial wave packet by a factor of 2 requires a factor of 4 more memory but, more importantly, a factor of 8 more CPU time (the additional factor of 2 comes from the fact that it takes twice as long for the wave packet to travel a distance which is twice as large).

By construction the norm of the wave function should be constant. Numerically, rounding errors lead to small deviations (recall the algorithm is stable under all circumstances) which are less than 10^{-8} in the present case. The energy $E=\langle \Phi(t) | \mathcal{H} | \Phi(t) \rangle$ and the spread on the energy $\langle \Phi(t) | \mathcal{H}^2 | \Phi(t) \rangle - E^2$ are constant up to at least 5 digits.

The final step is to analyze the wave packet transmitted by the two-slit arrangement. For the present purposes, it is not of great interest to compute the diffraction pattern at a screen placed near to the interferometer. Instead it is more appropriate to calculate the interference fringes on a screen at infinity. This can be done in the following way.⁵ After the scattering event has taken place, the transmitted (and also the reflected) wave packet moves in free space [for a vector potential of the form Eq. (2.1)]. Then the angular distribution of intensity $P(\theta)$ on the screen at infinity can be writ-

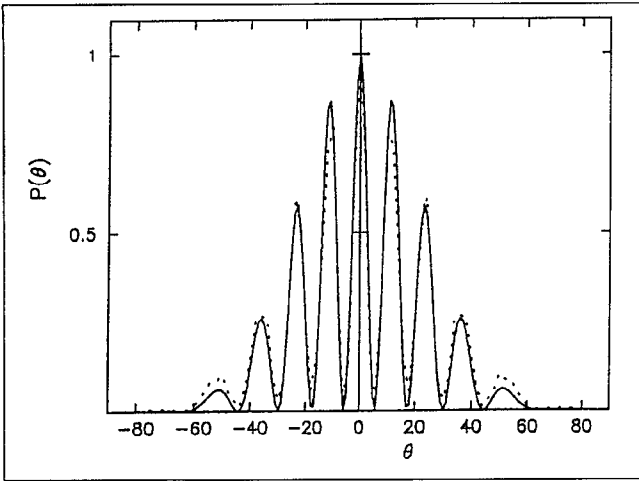


Figure 2. Diffraction pattern (dashed line) of a two-slit interferometer of dimensions $s=\lambda$ and $d=w=4\lambda$. The angle of incidence $\theta_0=0$. The magnetic field $B=0$. Solid line: theoretical result calculated from Eq. (2.7) with $\varphi=0$.

ten in terms of the Fourier transform of the transmitted wave packet.⁵ For the case at hand the normalized $P(\theta)$ is given by

$$P(\theta) = \frac{\int_0^\infty |\tilde{\Phi}(q_x, q_y=q_x \tan \theta, t=T)|^2 dq_x}{\int_0^\infty |\tilde{\Phi}(q_x, q_y=0, t=T)|^2 dq_x}, \quad (2.6)$$

where $|\tilde{\Phi}\rangle$ is the Fourier transform of $|\Phi\rangle$ and T is the time it takes for the transmitted wave packet to move freely (i.e., to propagate until there is no more scattering).

Some representative diffraction patterns of a two-slit interferometer of dimensions $s=\lambda$ and $d=w=4\lambda$ (see Fig. 1) are shown in Figs. 2–6 (dashed lines), for magnetic

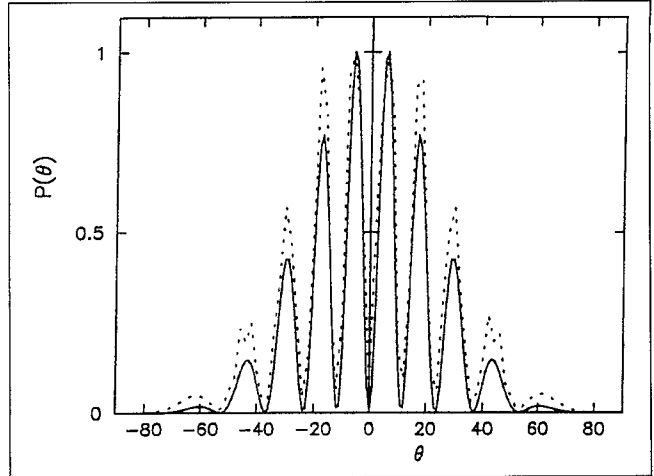


Figure 4. Diffraction pattern (dashed line) of a two-slit interferometer of dimensions $s=\lambda$ and $d=w=4\lambda$. The angle of incidence $\theta_0=0$. The magnetic field $B=B_0$. Solid line: theoretical result calculated from Eq. (2.7) with $\varphi=\pi$.

fields $B=0, B_0/2, B_0, 3B_0/2, 2B_0$, respectively. Also shown (solid lines) are the corresponding diffraction patterns calculated from

$$P(\theta) = \left\{ \frac{\sin[2d\pi(\sin \theta - \sin \theta_0) + \varphi]}{\sin[d\pi(\sin \theta - \sin \theta_0) + \varphi]} \right\}^2 \left\{ \frac{\sin(s\pi \sin \theta)}{s\pi \sin \theta} \right\}^2, \quad (2.7)$$

which, for zero magnetic field ($\varphi=0$), is *not* the Fraunhofer diffraction formula for two slits.¹ The difference is in the second factor where, compared to the Fraunhofer result, the dependence on the angle of incidence ($\sin \theta_0$) is missing. Numerous numerical experiments for two and multislit interferometers²⁷ of which the dimensions s and d are comparable to the wavelength λ lead to the conclusion that Eq. (2.7) provides a much better fit to the exact numerical re-

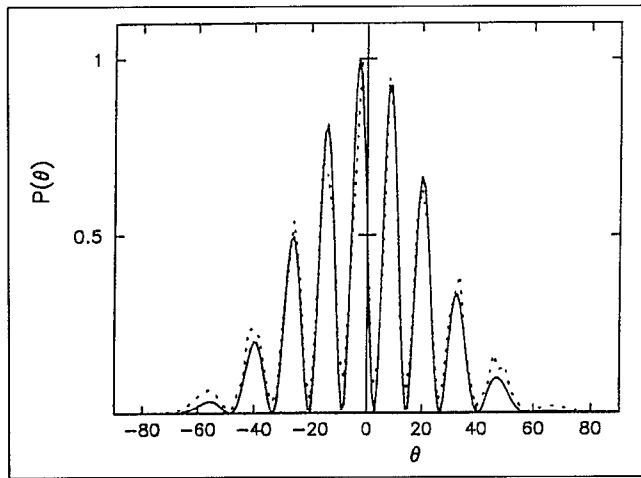


Figure 3. Diffraction pattern (dashed line) of a two-slit interferometer of dimensions $s=\lambda$ and $d=w=4\lambda$. The angle of incidence $\theta_0=0$. The magnetic field $B=B_0/2$. Solid line: theoretical result calculated from Eq. (2.7) with $\varphi=\pi/2$.

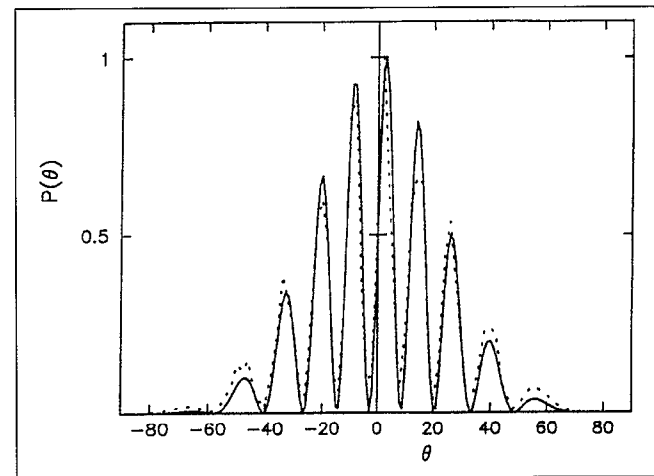


Figure 5. Diffraction pattern (dashed line) of a two-slit interferometer of dimensions $s=\lambda$ and $d=w=4\lambda$. The angle of incidence $\theta_0=0$. The magnetic field $B=3B_0/2$. Solid line: theoretical result calculated from Eq. (2.7) with $\varphi=3\pi/2$.

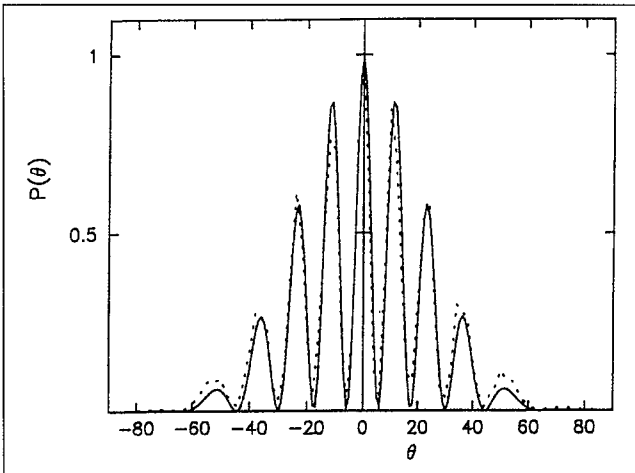


Figure 6. Diffraction pattern (dashed line) of a two-slit interferometer of dimensions $s=\lambda$ and $d=w=4\lambda$. The angle of incidence $\theta_0=0$. The magnetic field $B=2B_0$. Solid line: theoretical result calculated from Eq. (2.7) with $\varphi=2\pi$.

sults than the Fraunhofer expression does. As already mentioned in the Introduction, deviations from simple diffraction theory can be expected whenever the wavelength becomes comparable to the typical size of the scattering object and the numerical experiments presented here are clear-cut examples of this phenomenon.

From Figs. 3–6 it is also clear that even when the magnetic field is present, Eq. (2.7) remains in good qualitative agreement with the numerical data. At the same time, this yields a (numerical) proof of the existence of the *AB* effect in a regime where a semiclassical approach is not valid. Another proof, not relying on Eq. (2.7) is given in Fig. 7 where the diffraction patterns for $B=0$ (solid line) and $B=B_0$ (dashed line) are superimposed. According to *AB*,¹¹ maxima (minima) in the diffraction pattern for

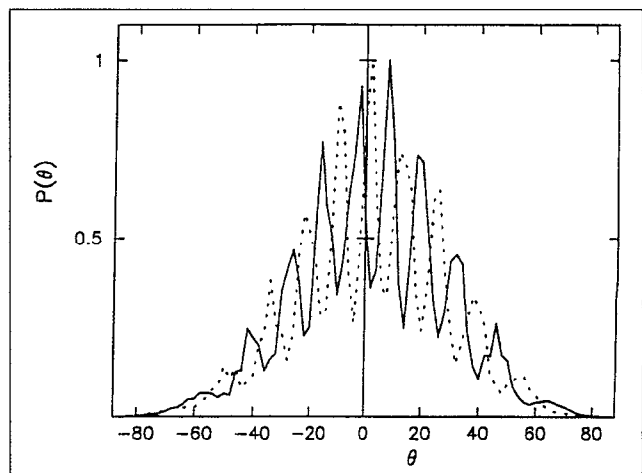


Figure 8. Diffraction patterns of a two-slit interferometer of dimensions $s=\lambda$ and $d=w=4\lambda$. The angle of incidence $\theta_0=\pi/9$. Solid line: magnetic field $B=0$. Dashed line: magnetic field $B=B_0$.

$B=B_0$ (or $\varphi=\pi$) should appear at the positions of the minima (maxima) in the diffraction pattern for $B=0$ and indeed, as shown in Fig. 7, this is the case.

All the results shown in Figs. 2–7 have been obtained using an initial wave packet with an angle of incidence of $\theta_0=0$. Some typical results for another angle of incidence ($\theta_0=\pi/9$) are shown in Fig. 8. Also these numerical results confirm the existence of the *AB* effect, as do similar calculations for other choices of θ_0 , s , d , and w (not shown). In addition, the results depicted in Fig. 8 provide a clear example where expression (2.7) is not a good approximation. Indeed, the minima of Eq. (2.7) correspond to zero intensity but in the exact solution this is definitely not the case (detailed inspection of the other figures confirms that this is a general feature). The fact that Eq. (2.7) can only be used to estimate the position of maxima and minima of the diffraction pattern is just another manifestation that simple diffraction theory cannot be employed if the dimensions of the interferometer are comparable to the wavelength of the incident wave.

ACKNOWLEDGMENTS

It is a pleasure to thank N. García and P. de Vries for stimulating discussions. This work is part of a research programme of the “Stichting voor Fundamenteel Onderzoek der Materie (FOM),” which is financially supported by the “Nederlandse Organisatie voor Wetenschappelijk Onderzoek (NWO).” Computer simulations were carried out in the context of a project of the “Stichting Nationale Computer Faciliteiten (NCF).” This work is partially supported by an EEC Human Capital and Mobility project.

REFERENCES

1. M. Born and E. Wolf, *Principles of Optics* (Pergamon, New York, 1959).
2. N. García, J. J. Sáenz, and H. De Raedt, *J. Phys.: Condens. Matter* 1, 9931 (1989).
3. H. De Raedt and K. Michielsen, *Nanosources and*

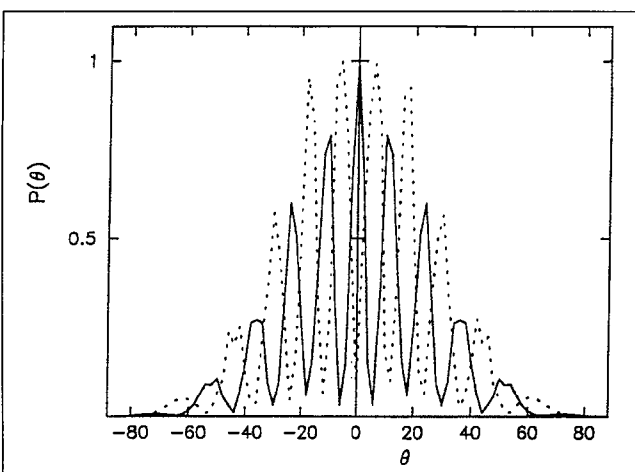


Figure 7. Diffraction patterns of a two-slit interferometer of dimensions $s=\lambda$ and $d=w=4\lambda$. The angle of incidence $\theta_0=0$. Solid line: magnetic field $B=0$. Dashed line: magnetic field $B=B_0$.

- Manipulation of Atoms Under High Fields and Temperatures: Applications*, NATO-ASI Series, edited by Vu Thien Binh, N. García, and K. Dransfeld (Kluwer, Dordrecht, 1993).
4. H. De Raedt, N. García, and J. Huyghebaert, Solid State Comm. **76**, 847 (1990).
 5. K. Michelsen and H. De Raedt, J. Phys.: Condens. Matter **3**, 8247 (1991).
 6. M. Suzuki, J. Math. Phys. **32**, 400 (1991).
 7. G. Baym, *Lectures on Quantum Mechanics* (Benjamin, Reading, MA, 1969).
 8. J. S. Townsend, *A Modern Approach to Quantum Mechanics* (McGraw-Hill, New York, 1992).
 9. P. J. E. Peebles, *Quantum Mechanics* (Princeton University, Princeton, NJ, 1992).
 10. B. R. Holstein, *Topics in Advanced Quantum Mechanics* (Addison-Wesley, Redwood City, CA, 1992).
 11. Y. Aharonov and D. Bohm, Phys. Rev. **115**, 485 (1959).
 12. D. H. Kobe, Ann. Phys. **123**, 381 (1979).
 13. H. De Raedt, Comp. Phys. Rep. **7**, 1 (1987).
 14. M. Suzuki, J. Math. Phys. **32**, 400 (1991).
 15. H. De Raedt, and B. De Raedt, Phys. Rev. A **28**, 3575 (1983).
 16. M. Suzuki, J. Math. Phys. **26**, 601 (1985).
 17. M. Abramowitz and I. A. Stegun, *Handbook of Mathematical Functions* (Dover, New York, 1964).
 18. The case $n=9$ is even simpler than the other eight cases but for the sake of brevity, a discussion of this detail is omitted.
 19. M. Peshkin, and A. Tonomura, *The Aharonov-Bohm Effect* (Springer, Berlin, 1989).
 20. Olariu and Popescu, Rev. Mod. Phys. **57**, 339 (1985).
 21. A. Tonomura, Adv. Phys. **41**, 59 (1992).
 22. A. Tonomura *et al.*, Phys. Rev. Lett. **48**, 1443 (1982).
 23. G. Badurek *et al.*, Phys. Rev. Lett. **71**, 307 (1993).
 24. M. Jursa, and P. Kasperkovitz, Phys. Rev. A **47**, 3602 (1993).
 25. R. A. Webb, S. Washburn, C. P. Umbach, F. P. Millican, R. B. Laibowitz, and A. B. Benoit, Physica A **140**, 175 (1986).
 26. I. V. Krive, and A. S. Roshavsky, Int. J. Mod. Phys. B **6**, 1255 (1992).
 27. K. Michelsen, and H. De Raedt, J. Phys.: Condens. Matter **34**, 7121 (1992).